

# Magnetization of carbonaceous asteroids by nebular fields and the origin of CM chondrites

**Samuel Courville** (✉ [swcourvi@asu.edu](mailto:swcourvi@asu.edu))

Arizona State University <https://orcid.org/0000-0002-9539-1301>

**Joseph O'Rourke**

Arizona State University <https://orcid.org/0000-0002-1180-996X>

**Julie Castillo-Rogez**

Jet Propulsion Laboratory, California Institute of Technology

**Roger Fu**

Harvard University

**Rona Oran**

Massachusetts Institute of Technology

**Benjamin Weiss**

MIT <https://orcid.org/0000-0003-3113-3415>

**Linda Elkins-Tanton**

Arizona State University

---

## Article

### Keywords:

**Posted Date:** January 12th, 2022

**DOI:** <https://doi.org/10.21203/rs.3.rs-1196868/v1>

**License:**  This work is licensed under a Creative Commons Attribution 4.0 International License.

[Read Full License](#)

---

**Version of Record:** A version of this preprint was published at Nature Astronomy on October 13th, 2022.

See the published version at <https://doi.org/10.1038/s41550-022-01802-z>.

1 **Magnetization of carbonaceous asteroids by nebular**  
2 **fields and the origin of CM chondrites**

3  
4 **Samuel W. Courville<sup>1\*</sup>, Joseph G. O'Rourke<sup>1</sup>, Julie C. Castillo-Rogez<sup>2</sup>, Roger R. Fu<sup>3</sup>, Rona**  
5 **Oran<sup>4</sup>, Benjamin P. Weiss<sup>4</sup>, Linda T. Elkins-Tanton<sup>1</sup>**

6  
7 <sup>1</sup>School of Earth and Space Exploration, Arizona State University, Tempe, AZ, USA,

8 <sup>2</sup>Jet Propulsion Laboratory, California Institute of Technology, Pasadena, CA, USA,

9 <sup>3</sup>Department of Earth and Planetary Sciences, Harvard University, Cambridge, MA, USA,

10 <sup>4</sup>Department of Earth, Atmospheric and Planetary Sciences, MIT, Cambridge, MA, USA

11

12 \*swcourvi@asu.edu

## 13 **Introductory Paragraph:**

14 The solar nebula carried a strong magnetic field that had a stable intensity and direction for  
15 periods of a thousand years or more<sup>1</sup>. The solar nebular field may have produced post-accretional  
16 magnetization in at least two groups of meteorites, CM and CV chondrites<sup>1-3</sup>, which originated  
17 from planetesimals that may have undergone aqueous alteration before gas in the solar nebula  
18 dissipated<sup>1,3</sup>. Magnetic minerals produced during aqueous alteration, such as magnetite and  
19 pyrrhotite<sup>4</sup>, could acquire a chemical remanent magnetization from that nebular field<sup>3</sup>. However,  
20 many questions about the size, composition, formation time, and, ultimately, identity of the  
21 parent bodies that produced magnetized CM and CV chondrites await answers—including  
22 whether a parent body might exhibit a detectable magnetic field today. Here, we use thermal  
23 evolution models to show that planetesimals that formed between a few Myr after CAIs and ~1  
24 Myr before the nebular gas dissipated could acquire from the nebular field, and retain until  
25 today, a chemical remanent magnetization throughout nearly their entire volume. Hence, in-situ  
26 magnetometer measurements of C-type asteroids could help link magnetized asteroids to  
27 magnetized meteorites. Specifically, a future mission could search for a magnetic field as part of  
28 testing the hypothesis that 2 Pallas is the parent body of the CM chondrites<sup>5</sup>. Overall, large  
29 carbonaceous asteroids might record ancient magnetic fields in magnetic remanence that  
30 produces strong modern magnetic fields, even without a metallic core that once hosted a  
31 dynamo.

32

## 33 **Main:**

34           Several meteorites in two groups of carbonaceous chondrites, the CM and CV chondrites,  
35 host a chemical remanent magnetization (CRM)<sup>3</sup> and possibly also thermoremanent  
36 magnetization<sup>6</sup>. CRM in a meteorite implies that chemical reactions produced ferromagnetic  
37 minerals within the meteorite's parent body while in the presence of a strong and temporally  
38 stable magnetic field. CM and CV chondrites experienced aqueous alteration, but little or no  
39 further dehydration or melting<sup>4</sup>. Aqueous alteration can produce minerals that are possible  
40 magnetic carriers<sup>4</sup>, such as magnetite (Fe<sub>3</sub>O<sub>4</sub>) and pyrrhotite (Fe<sub>(1-x)</sub>S, x=0 to 0.2). In general,  
41 ferromagnetic minerals forming in the presence of a background magnetic field can acquire a  
42 CRM in the same direction as the background field<sup>7,8</sup>. Thus, CRM in CM and CV chondrites  
43 indicates that their parent bodies may have undergone aqueous alteration in the presence of a  
44 strong magnetic field.

45

46           The magnetic field sustained by the cloud of dust and gas in the early solar nebula is  
47 likely the source of magnetization for the parent bodies of the CM chondrites<sup>3</sup>. Based on  
48 telescopic observations of distant solar nebulae and thermal remanent magnetization within  
49 chondrules of primitive LL and CO chondrites, the early solar nebula likely had a strong  
50 magnetic field that was active in the first few Myr of the solar system<sup>2,9-11</sup>. The nebula likely  
51 supported a strong magnetic field until at most ~3.9 Myr after CAIs in the inner solar system, or  
52 at most ~4.8 Myr in the outer solar system<sup>1</sup>. Thermal evolution models indicate whether  
53 planetesimals could experience aqueous alteration before the nebula dissipated—and thus  
54 whether planetesimals could acquire and retain magnetization from the nebular field.

55

56           During the heating of a planetesimal's interior through the radioactive decay of  $^{26}\text{Al}$ , two  
57 important thermal events determine the potential for acquiring a chemical remanent  
58 magnetization. First, the planetesimal reaches the melting point of water ice ( $\sim 273$  K). When  
59 water ice melts, liquid water drives aqueous alteration and produces the magnetic carriers  
60 magnetite and pyrrhotite<sup>4</sup>. If formed in the presence of the nebular magnetic field, these minerals  
61 acquire CRM. The second event occurs if the planetesimal reaches a maximum unblocking  
62 temperature, above which magnetized domains would randomize in zero-field conditions in a  
63 time less than the duration of peak heating (as short as  $\sim 10^2$  kyr). This maximum unblocking  
64 temperature, henceforth called the unblocking temperature, is different for each mineral, and also  
65 depends on geometric properties of individual grains such as size and shape<sup>12</sup>. Since these  
66 properties are stochastic and unknown a priori, we adopt fixed unblocking temperatures that are  
67 within empirically measured ranges<sup>3</sup>: 550 K for pyrrhotite and 850 K for magnetite (vs. Curie  
68 temperatures of 583 K and 858 K, respectively). If the planetesimal heats above the unblocking  
69 temperature(s) of its magnetic carrier(s) after the nebular magnetic field dissipates and stays  
70 above that temperature for longer than  $\sim 10^2$  kyr, then any magnetization in the minerals would  
71 be reset as the minerals re-magnetize in zero-background-magnetic-field conditions. If the  
72 planetesimal heats above, but then cools below the unblocking temperature(s) prior to the end of  
73 the lifetime of the nebula, then it will acquire a thermoremanence, possibly in addition to CRM.

74

75           An undisturbed planetesimal may experience one of three thermal evolution cases  
76 depending on the timing of the aforementioned milestones with respect to the lifetime of the  
77 solar nebular magnetic field. First, a planetesimal may form too late to reach the temperature to  
78 melt water ice before the solar nebula dissipates (Fig. 1a). This case results in no nebular

79 magnetization. Second, a planetesimal may form early enough to undergo aqueous alteration  
80 before the nebula dissipates but does not subsequently heat beyond the unblocking temperatures  
81 of magnetite or pyrrhotite (Fig. 1b). This scenario could lead to magnetization of nearly the  
82 entire planetesimal. Lastly, a planetesimal could form early enough to undergo aqueous  
83 alteration, but subsequently heat beyond the unblocking temperatures (Fig. 1c). Our models  
84 indicate that an undisturbed planetesimal (i.e., that did not experience impact unroofing and rapid  
85 cooling<sup>13</sup>) that heats beyond the unblocking temperature does not cool below that threshold again  
86 until many Myrs past when the nebula dissipates. Thus, such a planetesimal that reaches the  
87 unblocking temperature before the nebula dissipates would not retain magnetization throughout  
88 its interior. However, a thin shell of aqueously altered, chondritic material that does not reach the  
89 unblocking temperature could retain magnetization near the surface. Thus, magnetized CM  
90 chondrite meteorites could originate from either the second or third case. Only the second case  
91 could result in an asteroid with large-scale remanent magnetization from the solar nebula.

92  
93 Figure 2 plots the maximum volume percentage of a planetesimal that could be  
94 magnetized as a function of the planetesimal's radius and formation time. If the primary  
95 magnetic carrier is pyrrhotite, we find that a planetesimal may acquire large-scale magnetization  
96 from the solar nebula if it formed between  $\sim 3.5$  and  $3.7$  Myr after CAIs, depending on the exact  
97 timing of nebular dissipation (Fig. 2a). Since magnetite has a higher unblocking temperature,  
98 earlier forming planetesimals that reach hotter temperatures could still retain magnetization. If  
99 magnetite is abundant as a magnetic carrier, then we find that large-scale magnetization is  
100 possible for formation times between  $\sim 2.7$  and  $3.7$  Myr after CAIs (Fig. 2b). These ranges are  
101 consistent with the formation time expected for the parent bodies of the CM chondrites<sup>14</sup>.

102 Assuming that the entire volume of possible magnetization in each planetesimal model is  
103 coherently magnetized at the strength observed in the CM chondrites (see below for caveats),  
104  $\sim 10^{-4}$  A m<sup>2</sup>/kg, we plot the maximum possible magnetic dipole moment that each planetesimal  
105 might have today (Figs. 2c and 2d). For example, if Pallas formed at  $\sim 3.5$  Myr after CAIs, its  
106 maximum possible dipole moment now is  $\sim 10^{16}$  A m<sup>2</sup>. For comparison, Earth's magnetic  
107 moment is  $\sim 8 \times 10^{22}$  A m<sup>2</sup> and the metallic asteroid 16 Psyche may have a moment between  
108  $\sim 10^{15}$  A m<sup>2</sup> and  $10^{17}$  A m<sup>2</sup> if it is a disrupted planetary core<sup>15</sup>.

109

110 The maximum possible dipole moments displayed in Figs. 2c and 2d assume an idealistic  
111 scenario wherein the entire volume of the planetesimal has been magnetized unidirectionally.  
112 However, aqueous alteration need not occur homogeneously and contemporaneously throughout  
113 a planetesimal. If the solar nebular field's intensity and direction change between the time at  
114 which two different regions of a planetesimal experience aqueous alteration, then these two  
115 different regions would acquire different magnetization directions. The number and size of  
116 regions with differing magnetization strengths would depend on the rate of alteration compared  
117 to rate of field change. Additionally, impacts could scramble regions of coherent magnetization.  
118 The effective dipole moment of the planetesimal would be a function of the length scale of its  
119 magnetized regions. The smaller the length scale, the lower the effective dipole moment.

120

121 The asteroid 2 Pallas is a candidate parent body for the CM chondrites<sup>5</sup> because it  
122 exhibits a hydrated spectral signature in the 3- $\mu$ m region, which matches CM chondrite spectra<sup>16</sup>.  
123 Impacts can produce the observed differences between the visible and near-infrared spectra of  
124 Pallas and the CM chondrites<sup>5</sup>. Furthermore, the bulk density of Pallas ( $\sim 2.9$  g/cm<sup>3</sup>) is similar to

125 the grain density of CM chondrites<sup>17</sup>. Pallas also appears to lack a thick icy shell, based on its  
126 global morphology<sup>5</sup>, unlike Ceres. A possible model for Pallas' evolution is that it underwent  
127 aqueous alteration on a global scale and subsequently lost the remaining water ice as a  
128 consequence of subcatastrophic impacts, as suggested by the large basins found on its surface<sup>5,18</sup>.  
129 An early phase of hydrothermal evolution could limit heating and separation of a metallic core<sup>5</sup>.  
130 Based on our thermal evolution models, if Pallas is the parent body of the CM chondrites, then  
131 we expect it to be measurably magnetized.

132  
133 If the solar nebular field magnetized Pallas, then a spacecraft could possibly detect large-  
134 scale remanent fields that have persisted until today. To assess detectability, we estimate the  
135 magnetopause distance of a spherical asteroid with a radius of 256 km—the effective volume  
136 radius of Pallas<sup>5,19</sup>—orbiting at a distance of 2.8 AU in the present solar wind. Fig. 3 calculates  
137 the magnetopause distance as a function of the asteroid's effective magnetic dipole moment. This  
138 calculation generally agrees with magnetopauses numerically observed in hybrid simulations of  
139 asteroid magnetospheres in the solar wind<sup>20,21</sup>. For effective dipole moments above  $\sim 10^{13}$  to  $10^{14}$   
140 A m<sup>2</sup>, a spacecraft magnetometer flyby or orbiter could detect the asteroid's magnetosphere.  
141 Orbiters or landers could detect magnetization at smaller length scales. The exact minimum  
142 moment that is detectable depends on the specific mission design, and the orientation and  
143 interaction of the magnetized regions with the solar wind. Furthermore, low magnetic moments  
144 could also possibly be detected from orbit via the observation of Alfvén waves<sup>22</sup>.

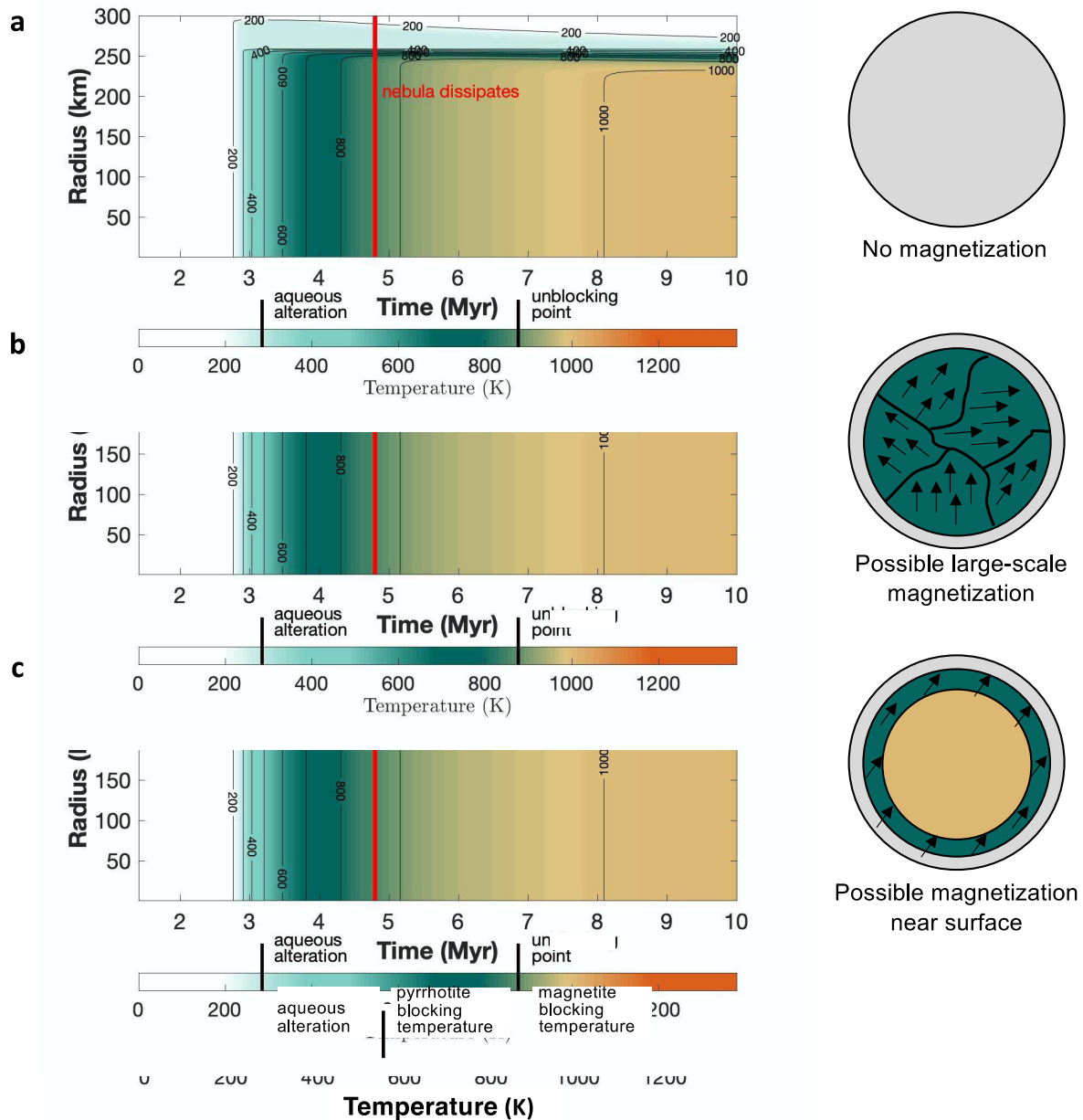
145  
146 The effective magnetic moment depends on the length scale of magnetization (Fig. 4).  
147 The length scale of a planetesimal's magnetic field depends on how aqueous alteration occurred

148 and whether the body has been disrupted by impacts throughout its lifetime. Different models of  
149 aqueous alteration predict various upper bounds for the length scales of magnetization (Fig. 4). If  
150 the distance over which fluid flows during the time that the solar nebular field is coherent  
151 determines the length scale, then the effective permeability of the planetesimal is the critical  
152 parameter. Assuming exhalation alteration (i.e., single-pass fluid flow directed to the surface<sup>23</sup>)  
153 and effective permeabilities between  $\sim 10^{-13}$  and  $10^{-12}$ , we expect magnetization length scales of  
154  $\sim 10$ – $100$  km. Alternatively, if aqueous alteration occurs over multiple-pass, pore-fluid  
155 convection, then the length and time scale of convection could determine the magnetization  
156 length scale. Pore-fluid and/or hydrothermal convection could have length scales of  $\sim 10$  km but  
157 requires a steep thermal gradient, which would only exist near the surface<sup>24,25</sup>. If alteration  
158 occurs as the result of effusive events of high temperature fluid and steam escaping the  
159 subsurface, i.e., a fumarolic system, then alteration would likely occur in distinct separate events  
160 and have scales of less than 10km, perhaps consistent with alteration environments in terrestrial  
161 ocean spreading centers<sup>26</sup>. For whole-body “mudball” convection<sup>27</sup>, the length scale could be as  
162 great as 100 km if alteration occurs homogeneously throughout convective cells within the  
163 mudball. Alternatively, aqueous alteration and the production of magnetic minerals may not be  
164 dependent on fluid flow, i.e., in models with isochemical alteration<sup>28</sup>. If ice and rock are  
165 homogeneously distributed throughout the body, and the body heats homogeneously, then large-  
166 scale, coherent magnetization could exist. The length scale of magnetization would represent that  
167 of any heterogeneous distribution of water ice, which would cause heterogeneity in the amount  
168 of radiogenic heating from the silicate component.

169

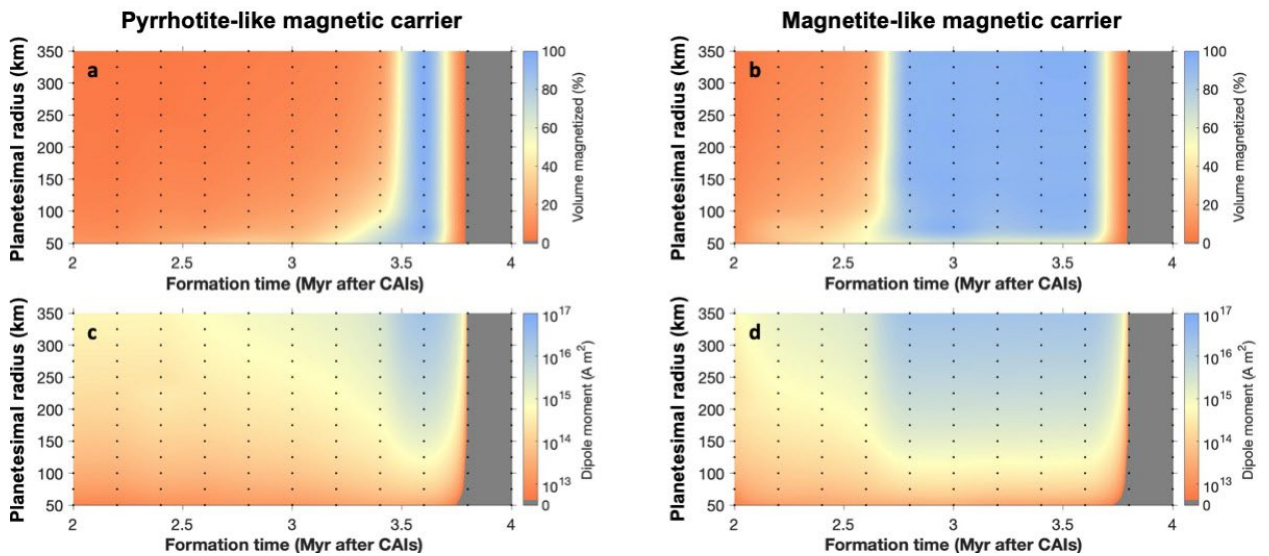
170 Overall, our work describes how a planetesimal that formed a few million years after  
171 CAIs would undergo enough heating to acquire a CRM during aqueous alteration while  
172 embedded within the solar nebular field, but not too much heating that would later erase the  
173 CRM. Additionally, our work establishes an upper bound on the magnetic dipole moment that is  
174 possible for a planetesimal magnetized by the solar nebula. We predict that large C-type  
175 asteroids that exhibit evidence of partial differentiation could have magnetospheres detectable  
176 from spacecraft. We hypothesize that Pallas is one such asteroid and show that this hypothesis  
177 can be tested with low-altitude, magnetic field measurements.

178



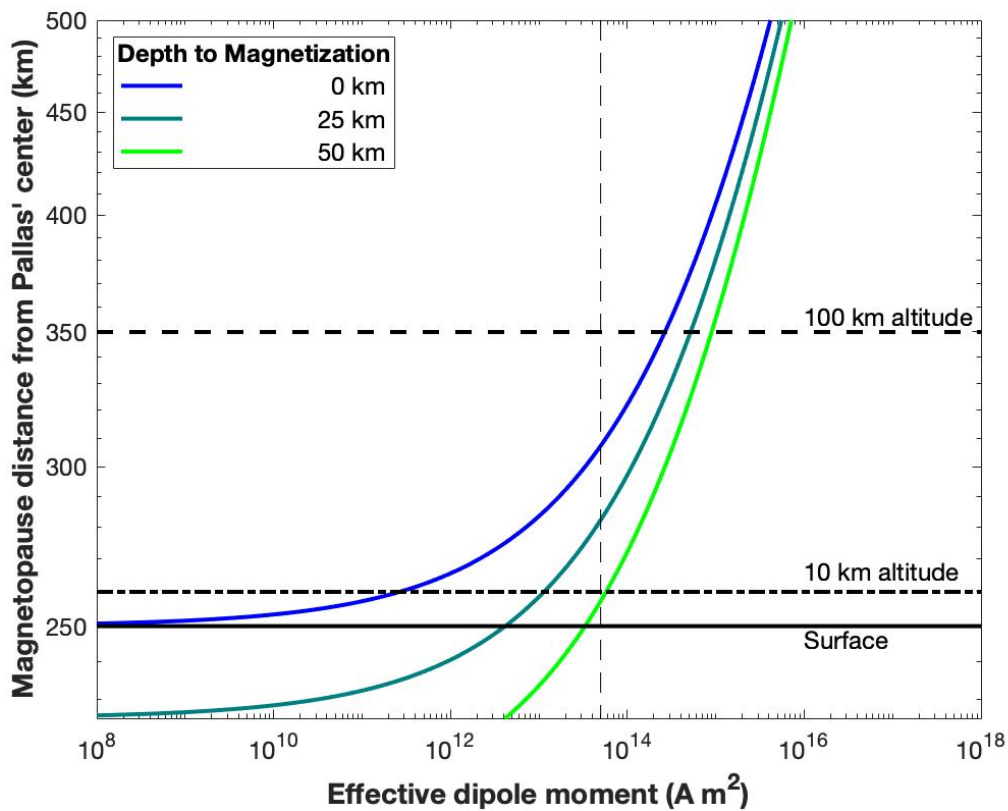
181 **Fig. 1: Planetesimal thermal evolution determines extent of aqueous alteration and thus**  
 182 **magnetizable volume.** Thermal evolution models for a 300-km-radius planetesimal assuming  
 183 formation at (a) 4 Myr, (b) 3.2 Myr, and (c) 2.8 Myr after CAIs. In panel (a), the planetesimal  
 184 forms too late for  $^{26}\text{Al}$ -driven heating to trigger aqueous alteration before the solar nebular field  
 185 dissipates. This case leads to no magnetization. In panel (b), the planetesimal forms early enough

186 for aqueous alteration to occur but does not subsequently exceed the unblocking temperatures of  
 187 the magnetic minerals. This scenario leads to possible coherent magnetization throughout the  
 188 entire body. In panel (c), the planetesimal heats enough to experience aqueous alteration before  
 189 the nebular field dissipates, but subsequently exceeds the unblocking temperature for most of the  
 190 interior. This evolution means that the majority of the planetesimal would be demagnetized  
 191 except for a thin shell near the surface.  
 192



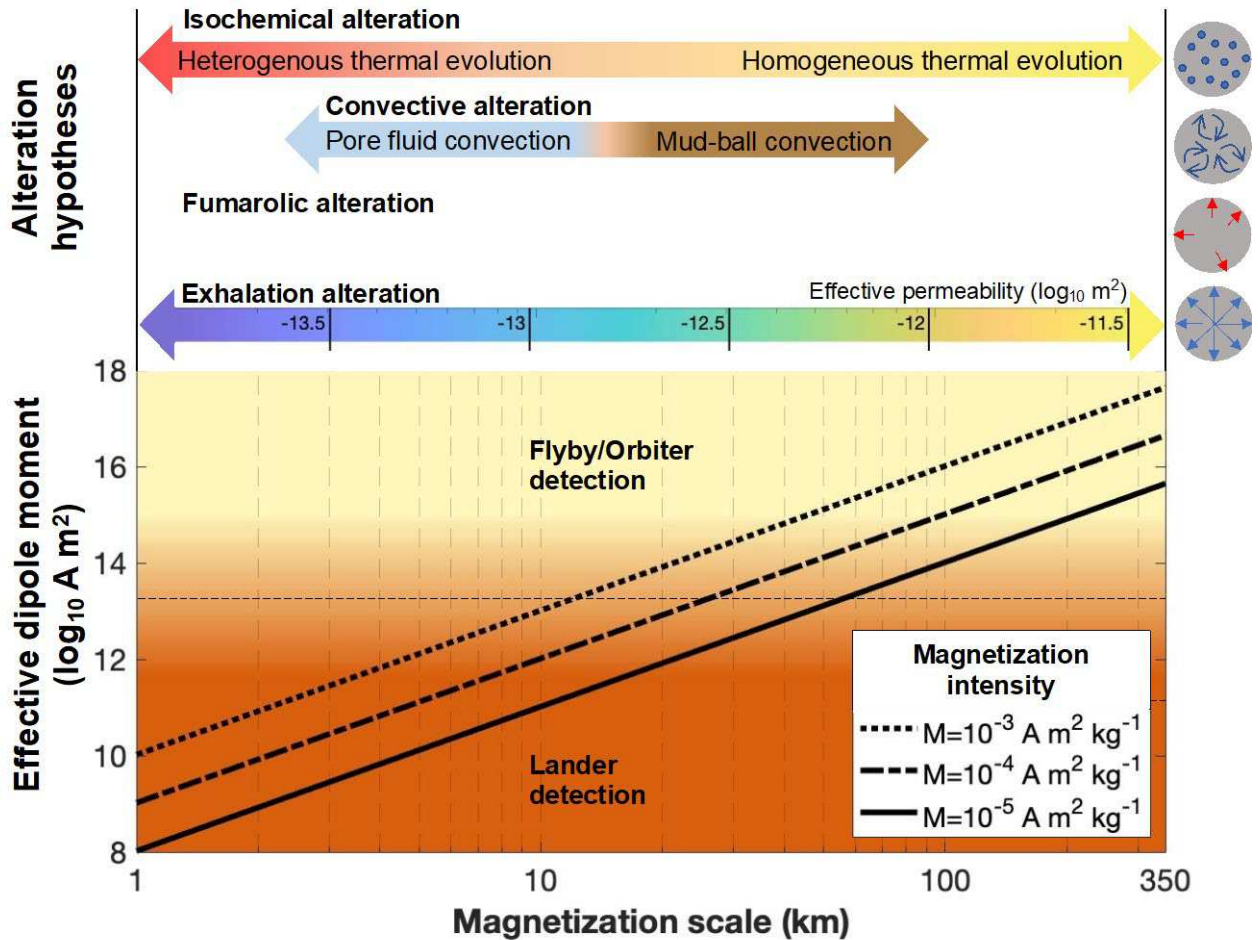
194 **Fig. 2: Formation time determines the maximum possible magnetized rock volume and**  
 195 **magnetic moment that a planetesimal could acquire.** Panels (a) and (b) illustrate the  
 196 maximum possible volume of the planetesimal that the solar nebular field could magnetize as a  
 197 function of the planetesimal's formation time and radius, assuming pyrrhotite and magnetite are  
 198 the magnetic carriers, respectively. A wide range of formation times lead to ~100%  
 199 magnetization if the magnetic carrier is magnetite. If the magnetic carrier is pyrrhotite, then the  
 200 extent of magnetization is more sensitive to formation time. Black dots represent individual  
 201 thermal model runs. We assume that the solar nebular field dissipated at 4.8 Myr after CAIs and

202 that the unblocking temperature is 550 K for pyrrhotite and 850 K for magnetite. The greater the  
 203 volume percentage of a planetesimal that is magnetized, the greater its magnetic dipole moment  
 204 could be. Panels (c) and (d) illustrate the maximum possible dipole moment where the magnetic  
 205 carrier is pyrrhotite and magnetite, respectively. Here we use a magnetization intensity of  $10^{-4}$  A  
 206  $\text{m}^2 \text{kg}^{-1}$ .  
 207



210  
 211 **Fig. 3: A magnetized chondritic asteroid can produce a detectable magnetopause.** The  
 212 curves represent the magnetopause distance as a function of a Pallas-sized asteroid's effective  
 213 magnetic dipole moment. The higher the magnetopause, the more easily detectable the asteroid's  
 214 magnetosphere. At low magnetic moments and close proximity to the asteroid's surface, the  
 215 magnetopause distance depends heavily on the depth to magnetization, with deeper

216 magnetization being more difficult to detect. Moments greater than  $\sim 10^{13}$  to  $10^{14}$  A m<sup>2</sup> are likely  
 217 detectable during an orbiter or flyby. Lower magnetic moments could be detected by a low orbit  
 218 or a lander. The exact cutoffs for detectability depend on specific mission parameters.  
 219



221 **Fig. 4: The aqueous alteration model determines the length scale of coherent remanent**  
 222 **magnetization, which determines the magnetic dipole moment.** We use three different  
 223 magnetization values corresponding to the range observed in CM chondrites<sup>3</sup>. The prevailing  
 224 aqueous alteration process determines the magnetization scale, which is the effective radius of  
 225 the volume that is coherently magnetized. Many aqueous alteration models exist. For outward

226 Darcy fluid flow (exhalation flow), effective permeability controls the magnetization length  
227 scale. If hydrothermal or fluid convection models control alteration, then the system or  
228 convection scale likely determines the magnetization scale. Lastly, alteration may not depend on  
229 fluid flow. In an isochemical model, the magnetization scale would depend on the homogeneity  
230 of the ice/rock ratio that controls thermal evolution. From Fig. 3, we expect that the lowest  
231 detectable dipole moment for an orbiter or flyby over the surface of Pallas is  $\sim 10^{13.5}$  A m<sup>2</sup>. Thus,  
232 it would be possible to detect magnetization from a spacecraft at Pallas if coherent magnetization  
233 exists at a scale greater than  $\sim 10$ –50 km.

234

## 235 **Acknowledgements:**

236 We thank Dr. Alan Rubin for fruitful discussion about the alteration of CM chondrites. BPW and  
237 RO thank the NASA Discovery Program (NNM16AA09 C) for support. Part of this work was  
238 carried out at the Jet Propulsion Laboratory, California Institute of Technology, under a contract  
239 with the National Aeronautics and Space Administration (80NM0018D0004).

## 240 **Methods:**

### 241 **Thermal evolution models:**

242 Thermal evolution controls how and when a planetesimal may acquire chemical remanent  
243 magnetization through aqueous alteration. We employ the thermal modeling algorithm described  
244 in Castillo-Rogez et al. (2007, 2010)<sup>29-31</sup>. This algorithm solves for the temperature profile at  
245 each radial extent,

$$246 \quad \frac{d\left(\frac{k(T)dT(r)}{dr}\right)}{dr} + \frac{2}{r}\left(\frac{k(T)dT(r)}{dr}\right) = \rho(r)C_p(T)\left(\frac{dT(r)}{dt}\right) - H(r),$$

247 where  $T$  is the temperature,  $r$  is the radius,  $k$  is the thermal conductivity,  $\rho$  is the density,  $C_p$  is  
248 the heat capacity, and  $H$  is the specific heat production from radiogenic decay. We assume the  
249 initial  $\text{Al}^{26}$  concentration is 600 ppb and that its specific heat production is 0.146 W/kg. The  
250 model time step is  $10^4$  years. Additionally, this thermal model includes heating from accretion,

$$251 \quad T(r) = \frac{h_a}{C_p(T)} \left[ \frac{4\pi}{3} \rho G r^2 + \frac{\langle v \rangle^2}{2} \right] + T_i,$$

252 where  $h_a$  is the fraction of mechanical energy transferred to heat,  $G$  is the gravitational constant,  
253  $v$  is the velocity of accreting objects, and  $T_i$  is the initial temperature. Even for the largest  
254 planetesimals we consider, the heat from accretion is only a few 10s of K, so the assumption of  
255 instantaneous accretion is acceptable. Full details of the model implementation, including the  
256 assumed values of all the parameters, are available in Castillo-Rogez et al. (2007)<sup>31</sup>.

257

258 We model an array of planetesimals with varying radii and formation time. Radii range  
259 from 50–350 km in increments of 25 km and formation times range from 2–4 Myr after CAIs in  
260 increments of 0.2 Myr. Additionally, we run each model with a starting water ice volume fraction

261 of 10 and 40%. We also run each model with initial temperatures of 100 and 160 K, which  
262 correspond to the expected outer (between the orbits of Jupiter and Uranus) and inner solar  
263 system temperatures respectively.

264

### 265 **Dipole moment calculation:**

266 The magnetic dipole moment is defined as,

$$267 \quad m = \iiint \mathbf{M} dV,$$

268 where  $\mathbf{M}$  is the magnetization and  $V$  is the magnetized volume. In general, an asteroid can be  
269 non-spherical, and the volume could be composed of fractions that have varying magnetization  
270 strengths and directions. To calculate the maximum possible dipole moment, we assume that the  
271 entire magnetized volume of the asteroid has the same magnetization direction. Additionally, we  
272 assume a radially symmetric asteroid. The dipole moment then simplifies to the product of the  
273 magnetization magnitude and the magnetized volume,

$$274 \quad m = MV.$$

275 The output of a planetesimal thermal model tells us what volume of the planetesimal can  
276 be magnetized. We assume that the magnetization value is  $10^{-4}$  A m<sup>2</sup>/kg, which falls within the  
277 range of values observed in CM chondrites<sup>3</sup>. One could attempt to calculate the magnetization of  
278 the planetesimal by assuming a nebular field strength and orientation, without relying on any  
279 meteoritic data. However, none of these parameters are constrained enough to provide a more  
280 precise estimate than our preferred method<sup>32,33</sup>.

281 Research suggests that the intensity and direction of the solar nebular field was likely  
282 stable for periods of  $\sim 1$  kyr or longer<sup>1</sup>—long enough to allow magnetic minerals to form during  
283 a planetesimal's aqueous alteration<sup>34</sup>. However, a rotating planetesimal orbiting around the early

284 Sun would have had an ever-changing orientation with respect to the nebular field. In this case,  
285 the planetesimal would acquire remanent magnetization in the net average direction of the  
286 background field parallel to the planetesimal's spin axis<sup>35</sup>. If the planetesimal's spin axis is not  
287 perfectly aligned with the disk plane, the projection of the spin axis onto the vertical component  
288 of the nebular field in the protoplanetary disk would have a non-zero average, as the vertical  
289 component would remain constant as the planetesimal orbits around the sun.

290 It is idealistic to assume that the solar nebula would magnetize an entire asteroid  
291 unidirectionally. If fluid flow from the core to the surface of a planetesimal drives the rate at  
292 which aqueous alteration occurs, the permeability of the planetesimal determines the length scale  
293 of magnetization. Under the assumption of Darcy fluid flow, the pressure gradient in the body  
294 drives fluid to the surface. The pressure gradient at a depth  $z$  is defined as,

$$295 \quad \frac{dP}{dz} = \rho g(z)$$

296 where  $\rho$  is density, and  $g$  is gravitational acceleration. The linear fluid velocity in a porous  
297 medium governed by Darcy's law follows the relationship,

$$298 \quad v(z) = \frac{k}{\mu\phi} \frac{dP}{dz}$$

299 where  $k$  is permeability,  $\mu$  is fluid viscosity, and  $\phi$  is porosity. Dividing the expected stability  
300 time of the nebular field,  $\sim 1$  kyr, by the velocity  $v$ , yields an estimate of the magnetization length  
301 scale. We report the length scale using the maximum fluid flow velocity within the body. The  
302 fluid viscosity of water is  $10^{-3}$  Pa s. Assuming the length scale corresponds to the radius of a  
303 spherical volume, the dipole moment is given by the product of the spherical volume and the  
304 magnetization value. At a spacecraft flyby distance (i.e., closest approach of  $\sim 100$  km or less  
305 from the surface of the planetesimal, depending on the mission design), a collection of randomly

306 oriented magnetized regions of similar size would produce a field strength that is approximately  
307 the same field strength as would come from the dipole moment of a single magnetized region.

308

309 **Magnetopause distance:**

310 To assess the detectability of a magnetized Pallas, we estimate the magnetopause distance. The  
311 magnetopause distance is the point at which the solar wind pressure and the asteroid's magnetic  
312 field pressure balance each other.

313 
$$D = R_p \left( \frac{f^2 B^2}{2\mu_0 m_H n V^2} \right)^{\frac{1}{6}}$$

314 where  $R_p$  is the radius of the body,  $m_H$  is the mass of a hydrogen ion,  $n = 2 \text{ cm}^{-3}$  is the density of  
315 the solar wind at the asteroid belt,  $V = 400 \text{ km/s}$  is the solar wind velocity, and  $f = 2$  is a  
316 geometric factor<sup>36</sup>.  $B$  is the field strength on the magnetic equator on the surface. For a magnetic  
317 dipole, the field strength is

318 
$$B = \frac{\mu_0}{2\pi} \frac{m}{R_m^3}$$

319 Where  $m$  is the magnetic moment, and  $R_m$  is the distance from the dipole center. This equation  
320 approximates the body's magnetic field as a dipole centered in the body. This approximation is  
321 valid for strong magnetic moments and magnetopause distances that are far from the surface of  
322 the body. However, small dipole moments as generated by groups of small length-scale dipoles  
323 would have a more complicated behavior at close distances. In this case, the surface field would  
324 be most dominated by the dipole that is closest. Thus, we plot the magnetopause distance  
325 assuming that the distance from the dipole center to the surface is the same as the length scale of  
326 the magnetization.

327

## 328 **Supplementary information:**

### 329 **Simulation assumptions and parameter uncertainties**

330 Figure 2 applies to planetesimals that formed in the outer solar system where the nebula  
331 dissipated<sup>1</sup> at a given time, in this case, 4.8 Myr. If the nebula dissipated sooner, then the range  
332 in formation times that could lead to large-scale magnetization would be narrower. Alternatively,  
333 a planetesimal is more likely to retain a CRM if the nebula dissipated later. Additionally, our  
334 thermal models assume that the planetesimals contain 40 vol% water ice. A lower water-to-rock  
335 ratio or higher concentration of <sup>26</sup>Al in the rock fraction would lead to faster heating and a  
336 narrower range of formation times that could result in large-scale, magnetization. If heating is  
337 sufficiently higher than our nominal scenario, large-scale magnetism dominated by pyrrhotite is  
338 not possible because a planetesimal would always exceed pyrrhotite's unblocking temperature.  
339 Extended Data Figs. 1 and 2 illustrate the effects of quicker nebular dissipation and a lower  
340 water-to-rock ratio, respectively.

341

342 The process of aqueous alteration occurs when water ice melts at 273 K. This assumes  
343 the ice fraction is pure water ice. In our thermal models, differentiation occurs instantaneously<sup>37</sup>.  
344 This assumption is valid because the timescale of water transport is likely much shorter than the  
345 timescale of the thermal evolution<sup>30,31</sup>. When the model reaches the water melting point, the  
346 water migrates toward the surface of the planetesimal. This time marks the point at which  
347 aqueous alteration occurs throughout the planetesimal. Our results are largely independent of  
348 planetesimal size for radii greater than ~50 km. For smaller planetesimals, the amount of  
349 volumetric radiogenic heat generated versus heat lost radiating from the surface becomes an  
350 important factor. However, the thermal models are only accurate for diameters greater than

351 approximately 50 km; below this diameter, the assumption of instantaneous differentiation  
352 leading to the migration of liquid water to the surface is no longer valid. The models are  
353 computed accurately under the assumption that the differentiated body has a rocky mantle and  
354 water layer. From a thermal evolution standpoint, these models are upper bounds on the max  
355 temperature achieved.

356

357         Lastly, our modeling assumes that planetesimals instantaneously accreted unaltered  
358 material (i.e., no alteration during accretion) and that no disruption occurred to the planetesimal  
359 during its thermal evolution. Although C-type asteroids could have accreted material that was  
360 already aqueous altered to begin with<sup>14</sup>, this assumption would not alter our conclusions so long  
361 as additional alteration could take place. The assumption of instantaneous accretion is acceptable  
362 because under the paradigm of pebble accretion, planetesimals likely formed quickly relative to  
363 the timescale of radiogenic heating<sup>38</sup>. Instabilities in the protoplanetary disc could bring together  
364 bodies on the order of 10s–100s of km over kyrs<sup>33</sup>. Indeed, the theory of planet formation by  
365 pebble accretion requires a large reservoir of planetesimals of this size which could subsequently  
366 grow into protoplanets by continuing aggregation of dust and pebbles. However, alteration  
367 during protracted accretion or catastrophic disruptions may still have occurred which we do not  
368 consider<sup>39</sup>.

369

370

### 371 **Alternative origins of magnetization in planetesimals**

372         Parts of a planetesimal that undergo aqueous alteration could acquire magnetization from  
373 either an endogenous or exogenous magnetic field. An endogenous field origin requires that the

374 planetesimal once hosted a dynamo, presumably in a metallic core that is vigorously convecting  
375 due to rapid cooling. Therefore, a planetesimal can only host a dynamo if it heated up enough to  
376 melt metal and form a liquid core. Chondrites are undifferentiated material; however, they may  
377 originate from the outermost shells of parent bodies that are internally differentiated. That is,  
378 some chondritic material may remain relatively cold near the surface of a differentiated body<sup>40,41</sup>  
379 but experience an endogenous magnetic field from a core dynamo in the hot interior<sup>42</sup>. In other  
380 words, steep thermal gradients in the outermost layers of a parent body could keep the exterior  
381 cool even if the interior is relatively hot.

382

383       Formation of a metallic cores can occur as early as a few Myr after CAIs for bodies that  
384 formed early in the history of the solar system with scant water ice<sup>40</sup>. However, studies of  
385 asteroid dynamos suggest that the onset of a magnetic field would not occur until ~5 Myr after  
386 CAIs or later<sup>40,42</sup> because the core needs to start cooling to kickstart a dynamo. Radiogenic  
387 dating of carbonate minerals associated with aqueous alteration in CM chondrites places their  
388 formation time between ~2.4 and 4 Myr after CAIs<sup>43</sup>. Based on alteration sequences proposed for  
389 CM chondrites, these minerals likely formed contemporaneously with pyrrhotite and  
390 magnetite<sup>2,44</sup>. Thus, it is unlikely that an endogenous magnetic field from a core dynamo  
391 magnetized the CM chondrites if model-predicted dynamo timing and the ages of the CM  
392 magnetized minerals are correct.

393

394       A spacecraft detection of a magnetosphere around Pallas would add evidence to the  
395 hypothesis that Pallas is a possible parent body for the CM chondrites, assuming that the  
396 spacecraft could also rule out the presence of a large metallic core. The absence of a metallic

397 core would rule out a dynamo origin for the magnetization. Measurements of the density of the  
398 near-surface material, compared to the bulk density and (if available) the moment of inertia,  
399 would help determine the extent of internal differentiation. Knowledge of the internal  
400 differentiation state could constrain whether a metallic core may exist to host a dynamo source<sup>42</sup>.  
401 Additionally, the magnetization could not be confused with accretional-detrital-remanent  
402 magnetization<sup>45</sup>. Accretional-detrital-remanent magnetization is produced by magnetized grains  
403 aligning themselves during the process of accretion in the solar nebular field. However, this  
404 magnetization process would not produce coherent magnetization above the meter-scale<sup>45</sup>, and  
405 thus only a magnetometer landed on the surface of an asteroid could detect accretional-detrital-  
406 remanent magnetization. Thus, observations of large-scale magnetization on Pallas combined  
407 with the absence of a core would uniquely confirm that it formed before the solar nebular  
408 dissipated.

409

410 In principle, a strong solar wind—as opposed to the solar nebular field—could magnetize  
411 parts of planetesimals. Although the early solar wind was stronger than the solar wind today, it  
412 was probably still too weak to magnetize chondritic material<sup>35</sup>. Nevertheless, one recent study<sup>46</sup>  
413 suggested that the early solar wind could magnetize planetesimals because young planetesimals  
414 would behave more like comets and have conductive outer shells that could amplify the  
415 magnetizing field by an order of magnitude near the surface. In this scenario, CM chondrites  
416 could originate from the magnetized outer shell of a planetesimal. Whether magnetization by the  
417 solar wind could produce a planetesimal with a magnetized shell remains controversial<sup>35</sup>. In any  
418 case, the solar wind is not expected to produce planetesimal with large-scale magnetization.

419 Again, observations of a strong remanent magnetization could reveal the timing of the formation  
420 of planetesimals like Pallas.

421

### 422 **Length scale of magnetization**

423 The rate of fluid flow in planetesimals could have controlled the rate of mineral  
424 alteration<sup>23</sup>. In this case, the greater the permeability of the planetesimal, the greater the length  
425 scale of magnetization. The permeability of a planetesimal at early times is difficult to determine.  
426 Estimates<sup>25,28</sup> based on geodynamical arguments and/or measurements of meteorites and  
427 terrestrial analogs range widely from  $\sim 10^{-19}$  to  $10^{-11}$  m<sup>2</sup>. Measurements of permeability in  
428 meteorite samples tend to favor low permeability values<sup>28,47</sup>; however, geodynamical models of  
429 aqueous alteration often assume high permeability<sup>25,48</sup>. These need not be in complete agreement.  
430 Although the permeability of a meteorite hand sample is low, the overall effective permeability  
431 of a planetesimal could be much greater due to large fractures and fluid conduits<sup>24</sup> or because the  
432 material has not yet been lithified<sup>23</sup>. If the effective permeability is high, then fluid could flow  
433 quickly from the planetesimal's interior to its surface in kyrs, i.e., exhalation flow<sup>49</sup>. Quick  
434 exhalation flow could produce large-scale, coherent magnetization of potentially the entire  
435 planetesimal body. Per contra, fast exhalation flow might not allow enough time for chemical  
436 reactions to occur<sup>49</sup>. Multiple pass fluid flow, e.g., pore fluid convection, may be required to  
437 produce the degree of aqueous alteration seen in CM chondrites<sup>50</sup>. Near the surface of a  
438 planetesimal, fluid flow could be dominated by convection<sup>25</sup>. The thermal gradient near the  
439 surface would cause warm water to rise while cold water descends. Under this regime, we would  
440 expect the magnetization length scale would be approximately the convection length scale.  
441 Modeling of pore fluid convection indicates scales of  $\sim 10$  km. Lastly, high temperature

442 hydrothermal systems may occur within planetesimals<sup>51</sup>. High temperature hydrothermal  
443 reactions in fumarolic-like systems that involve effusive events of steam are potentially able to  
444 alter minerals much more quickly (10s of yrs or less) than conventional fluid alteration<sup>34</sup>.  
445 However, fumarolic alteration would be limited to small, localized regions. From terrestrial  
446 analogs<sup>52</sup>, we expect this length scale would be on the order of 1–10 km.

447  
448 If the permeability of a planetesimal is as low as  $10^{-19}$  m<sup>2</sup>, then fluid flow would be so  
449 slow that effectively all aqueous alteration would occur with stagnant and chemically isolated  
450 water<sup>28</sup>. This model matches geochemical studies of CM chondrites which indicate alteration  
451 occurred isochemically<sup>25,28</sup>. In the previous paragraph, we implicitly assume that the length scale  
452 of magnetization would be determined by the distance that fluid can travel over the period of  
453 nebular field stability (~1 kyr). However, aqueous alteration that occurs from chemically isolated  
454 fluids would produce magnetization length scales that depend on the homogeneity of internal  
455 heating. If water ice is distributed homogeneously throughout the planetesimal's body, then we  
456 would expect most of the interior to reach the ice melting point around the same time. At this  
457 point, all rock would be exposed to at least a little water which may or may not be trapped.  
458 Under this assumption, the magnetization length scale then depends on how homogeneously the  
459 body heats, which is dependent on how homogeneously the water ice and radiogenic isotopes are  
460 distributed. In the absence of constraints, this could lead to any length scale value.

461  
462 Finally, debates over permeability and whether alteration was isochemical can be  
463 bypassed altogether if aqueous alteration occurred in un-lithified rock. In this case, water melting  
464 leads to a muddy mixture of mobile pebbles<sup>27</sup>. Since both the pebbles and the fluid are well

465 mixed and mobile, a muddy planetesimal may experience “mudball” convection, wherein both  
466 solids and fluid move about the asteroid in order to dissipate heating<sup>27,53</sup>. This whole-body  
467 convection can extend from the mud-mantle to the core. The sorting of particle sizes and variable  
468 water-to-rock ratio throughout a convecting mudball would lead to compositional heterogeneity  
469 over short length scales<sup>27</sup>. We expect that magnetization length scales would be on the order of  
470 ~10–100 km based on the size of convective cells.

471

472         To summarize, if exhalation flow dominates the magnetic length scale, then the scale  
473 would be determined by the permeability of the body. Under the assumption of permeable  
474 material, we expect magnetization scales to be on the order of 10–100 km. Under the realm of  
475 fluid convection dominated alteration, we expect that only the near surface within kms of the  
476 surface would have the temperature gradient necessary to sustain convection, so length scales  
477 would be ~10 km. If fumarolic systems dominate magnetization, then based on terrestrial  
478 hydrothermal scales, the length scale could be on the order of 1–10 km. If the asteroid is not  
479 permeable, then alteration scales could take on a wide range of values depending on the  
480 homogeneity of temperature increase throughout the body (e.g., from <1 km to > 100km).  
481 Finally, “mudball” convection could lead to magnetization length scales of up to 100 km.

482

### 483 **Constraints from spacecraft observations**

484         To date, only one spacecraft with a magnetometer has visited a C-Type asteroid. The  
485 MASCOT lander aboard JAXA’s Hayabusa2 mission made magnetic field measurements on the  
486 surface of the C-type, rubble-pile asteroid (162173) Ryugu<sup>54</sup>. However, the MASCOT lander did  
487 not detect a magnetic field intrinsic to Ryugu<sup>54</sup>. This means that if Ryugu has magnetization, it

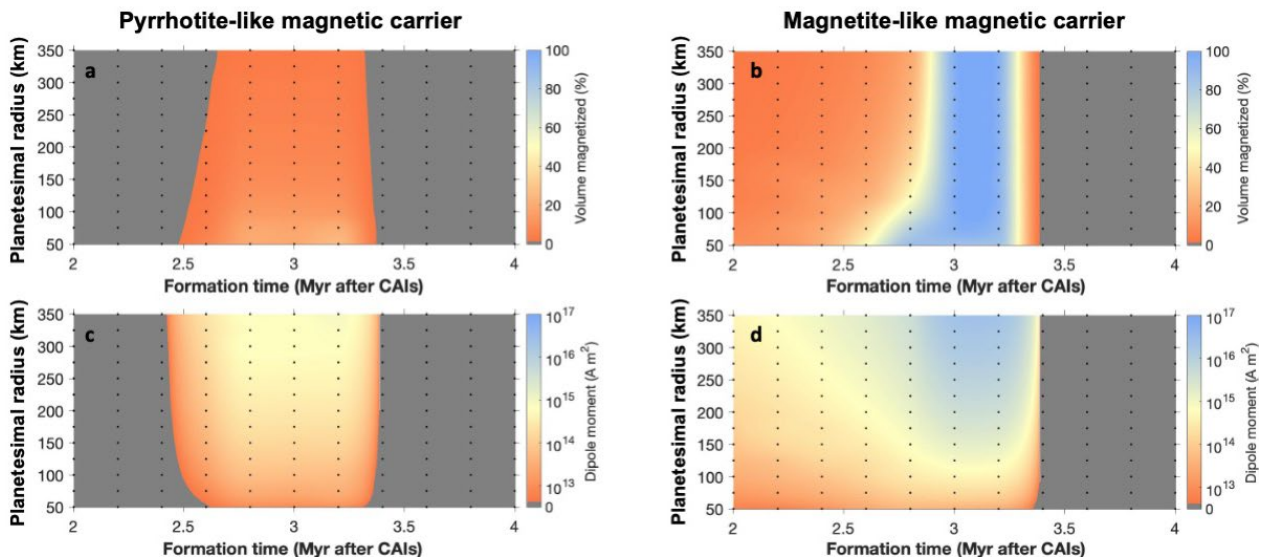
488 must be at a scale less than 1 cm<sup>54</sup>. This does not preclude the possibility of magnetized C-type  
489 asteroids. First, Ryugu is a rubble pile, so strong coherent magnetization is not possible as any  
490 magnetized pebbles or boulder would have scrambled orientations. Furthermore, Ryugu's  
491 composition may not match that of aqueously altered chondrites, and thus are not applicable to  
492 this study. However, if samples from Ryugu do match CM chondrites for example, and do not  
493 have any detectable magnetization or evidence that magnetization could have been erased, then  
494 this would suggest that magnetization of CM chondrites is not a ubiquitous process occurring  
495 throughout the entire body of an original CM chondrite parent body. Preliminary publications  
496 suggest Ryugu is more like CI chondrites<sup>55</sup>.

497

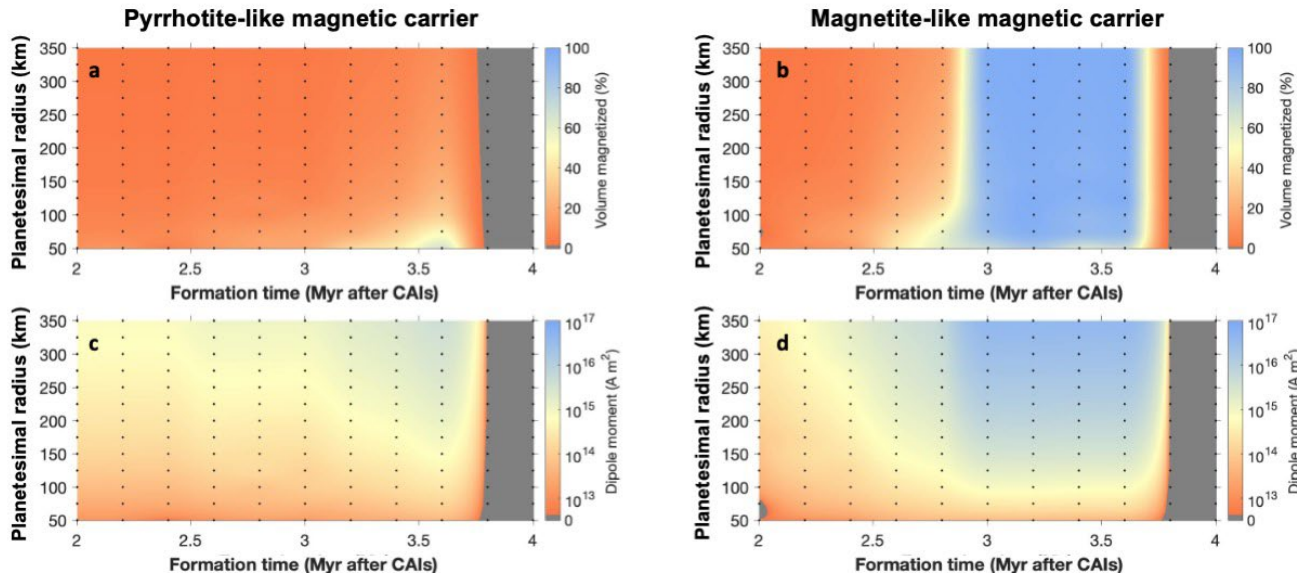
498         Although NASA's Dawn spacecraft did not have a magnetometer, Dawn did visit the  
499 largest C-type asteroid, 1 Ceres. Using observations from the Gamma Ray and Neutron Detector  
500 (GRaND), one can place an upper limit on Ceres' magnetic field by analyzing the deflection of  
501 charged particles<sup>56</sup>. Although GRaND made transient detections of deflected particles, it did not  
502 observe a signal consistent with a bow shock from a strong dipolar field in the solar wind<sup>56</sup>.  
503 Through this argument, Ceres cannot have a magnetic moment greater than  $\sim 10^{16}$  A m<sup>2</sup> or so<sup>56</sup>.  
504 This limit does not rule out large-scale, coherent magnetization, so we cannot exclude the  
505 possibility that Ceres has a detectable CRM from the solar nebular field.

506

507 **Extended Data Figures:**



509 **Extended Data Figure 1:** Maximum magnetized volume percent for planetesimals with 40 vol%  
510 water ice that formed in the inner solar system where the solar nebula dissipated at 3.9 Myr after  
511 CAIs and assuming an unblocking temperature of (a) 550 K and (b) 850 K, which correspond to  
512 the magnetic carriers pyrrhotite and magnetite respectively. Panels (c) and (d) illustrate the  
513 maximum possible dipole moment corresponding to panels (a) and (b) respectively. Quicker  
514 nebula dissipation leads to fewer planetesimals that could be magnetized. Compared to the  
515 nominal case in Fig. 2, the range of time that can lead to 100% magnetization has been greatly  
516 reduced if magnetite is the carrier and eliminated if pyrrhotite is the carrier.



518 **Extended Data Figure 2:** Maximum magnetized volume percent for planetesimals with 10 vol%  
 519 water ice that formed in the outer solar system where the solar nebula dissipated at 4.8 Myr after  
 520 CAIs and assuming an unblocking temperature of (a) 550 K and (b) 850 K, which corresponds to  
 521 the magnetic carrier being pyrrhotite and magnetite respectively. Panels (c) and (d) illustrate the  
 522 maximum possible dipole moment corresponding to panels (a) and (b) respectively. Because  
 523 there is less water ice, there is more radiogenic heating. More radiogenic heating means it is  
 524 easier to reach the unblocking temperature(s) and erase magnetization. Compared to the nominal  
 525 case in Fig. 2, the range in time that allows for 100% magnetization assuming magnetite is the  
 526 magnetic carrier has been narrowed. No times allow 100% magnetization assuming pyrrhotite is  
 527 the carrier. A 10 vol% water ice planetesimal would not have enough water to undergo complete  
 528 aqueous alteration, and low water content is not likely in the outer solar system. Furthermore,  
 529 even if it did occur, magnetite and pyrrhotite may not form, as hematite and tochilinite could be  
 530 the preferred minerals. Regardless, this scenario illustrates that models incorporating lower water  
 531 ice, or greater heating from a higher  $^{26}\text{Al}$  abundance, are less favorable for large scale  
 532 magnetization.

533

## 534 **References:**

- 535 1. Weiss, B. P., Bai, X.-N. & Fu, R. R. History of the solar nebula from meteorite  
536 paleomagnetism. *Sci. Adv.* **7**, eaba5967 (2021).
- 537 2. Fu, R. R. *et al.* The Fine-Scale Magnetic History of the Allende Meteorite: Implications  
538 for the Structure of the Solar Nebula. *AGU Adv.* **2**, 1–21 (2021).
- 539 3. Cournede, C. *et al.* An early solar system magnetic field recorded in CM chondrites. *Earth*  
540 *Planet. Sci. Lett.* **410**, 62–74 (2015).
- 541 4. Rubin, A. E., Trigo-Rodríguez, J. M., Huber, H. & Wasson, J. T. Progressive aqueous  
542 alteration of CM carbonaceous chondrites. *Geochim. Cosmochim. Acta* **71**, 2361–2382  
543 (2007).
- 544 5. Marsset, M. *et al.* The violent collisional history of aqueously evolved (2) Pallas. *Nat.*  
545 *Astron.* (2020) doi:10.1038/s41550-019-1007-5.
- 546 6. Carporzen, L. *et al.* Magnetic evidence for a partially differentiated carbonaceous  
547 chondrite parent body. *Proc. Natl. Acad. Sci.* **108**, 6386 LP – 6389 (2011).
- 548 7. Stacey, F. D. & Banerjee, S. K. Chemical Remanent Magnetization (CRM). *Part Vol.*  
549 *Phys. Princ. Rock Magn.* 128–135 (1974) doi:10.1016/b978-0-444-41084-9.50013-8.
- 550 8. Stacy, F. D. Paleomagnetism of meteorites. *Annu. Rev. Earth Planet. Sci.* **4**, 147–157  
551 (1976).
- 552 9. Symington, N. H., Harries, T. J., Kurosawa, R. & Naylor, T. T Tauri stellar magnetic  
553 fields: He I measurements. *Mon. Not. R. Astron. Soc.* **358**, 977–984 (2005).
- 554 10. Fu, R. R. *et al.* Solar nebula magnetic fields recorded in the Semarkona meteorite. *Science*  
555 (80-. ). **346**, 1089–1092 (2014).

- 556 11. Borlina, C. S. *et al.* Paleomagnetic evidence for a disk substructure in the early solar  
557 system. *Sci. Adv.* **7**, eabj6928 (2021).
- 558 12. Lowrie, W. Identification of ferromagnetic minerals in a rock by coercivity and  
559 unblocking temperature properties. *Geophys. Res. Lett.* **17**, 159–162 (1990).
- 560 13. Ciesla, F. J., Davison, T. M., Collins, G. S. & O’Brien, D. P. Thermal consequences of  
561 impacts in the early solar system. *Meteorit. Planet. Sci.* **48**, 2559–2576 (2013).
- 562 14. Desch, S. J., Kalyaan, A. & Alexander, C. M. O. The Effect of Jupiter’s Formation on the  
563 Distribution of Refractory Elements and Inclusions in Meteorites. *Astrophys. J. Suppl. Ser.*  
564 **238**, 11 (2018).
- 565 15. Elkins-Tanton, L. T. *et al.* Observations, Meteorites, and Models: A Preflight Assessment  
566 of the Composition and Formation of (16) Psyche. *J. Geophys. Res. Planets* **125**, 1–23  
567 (2020).
- 568 16. Larson, H. P., Feierberg, M. A. & Lebofsky, L. A. The composition of asteroid 2 Pallas  
569 and its relation to primitive meteorites. *Icarus* **56**, 398–408 (1983).
- 570 17. Macke, R. J., Consolmagno, G. J. & Britt, D. T. Density, porosity, and magnetic  
571 susceptibility of carbonaceous chondrites. *Meteorit. Planet. Sci.* **46**, 1842–1862 (2011).
- 572 18. Schmidt, B. E. & Castillo-Rogez, J. C. Water, heat, bombardment: The evolution and  
573 current state of (2) Pallas. *Icarus* **218**, 478–488 (2012).
- 574 19. Carry, B. *et al.* Physical properties of (2) Pallas. *Icarus* **205**, 460–472 (2010).
- 575 20. Blanco-Cano, X. & Omid, N. Hybrid simulations of solar wind interaction with  
576 magnetized asteroids: Comparison with Galileo observations near Gaspra and Ida. *J.*  
577 *Geophys. Res. Sp. Phys.* **108**, 1–13 (2003).
- 578 21. Fatemi, S., Poppe, A. R., Delory, G. T. & Farrell, W. M. AMITIS: A 3D GPU-Based

- 579 Hybrid-PIC Model for Space and Plasma Physics. *J. Phys. Conf. Ser.* **837**, (2017).
- 580 22. Unti, T. W. J. & Neugebauer, M. Alfvén Waves in the Solar Wind. *Phys. Fluids* **11**, 563–  
581 568 (1968).
- 582 23. Young, E. D., Ash, R. D., Philip, E. & Douglas, R. Fluid Flow in Chondritic Parent  
583 Bodies: Deciphering the Compositions of Planetesimals. *Science (80-. )*. **286**, 1331–1335  
584 (1999).
- 585 24. Kaplan, H. H. *et al.* Bright carbonate veins on asteroid (101955) Bennu: Implications for  
586 aqueous alteration history. *Science (80-. )*. **370**, eabc3557 (2020).
- 587 25. Young, E. D., Zhang, K. K. & Schubert, G. Conditions for pore water convection within  
588 carbonaceous chondrite parent bodies – implications for planetesimal size and heat  
589 production. *Earth Planet. Sci. Lett.* **213**, 249–259 (2003).
- 590 26. Jamieson, J. W. *et al.* Sulfide geochronology along the Endeavour Segment of the Juan de  
591 Fuca Ridge. *Geochemistry, Geophys. Geosystems* **14**, 2084–2099 (2013).
- 592 27. Bland, P. A. & Travis, B. J. Giant convecting mud balls of the early solar system. *Sci.*  
593 *Adv.* **3**, e1602514 (2021).
- 594 28. Bland, P. A. *et al.* Why aqueous alteration in asteroids was isochemical: High  
595 porosity≠high permeability. *Earth Planet. Sci. Lett.* **287**, 559–568 (2009).
- 596 29. Castillo-Rogez, J. C. & Schmidt, B. E. Geophysical evolution of the Themis family parent  
597 body. *Geophys. Res. Lett.* **37**, 1–5 (2010).
- 598 30. Castillo-Rogez, J. C. & McCord, T. B. Ceres’ evolution and present state constrained by  
599 shape data. *Icarus* **205**, 443–459 (2010).
- 600 31. Castillo-Rogez, J. C. *et al.* Iapetus’ geophysics: Rotation rate, shape, and equatorial ridge.  
601 *Icarus* **190**, 179–202 (2007).

- 602 32. Wardle, M. Magnetic fields in protoplanetary disks. *Astrophys. Space Sci.* **311**, 35–45  
603 (2007).
- 604 33. Johansen, A. & Lambrechts, M. Forming Planets via Pebble Accretion. *Annu. Rev. Earth  
605 Planet. Sci.* **45**, 359–387 (2017).
- 606 34. Ganino, C. & Libourel, G. Fumarolic-like activity on carbonaceous chondrite parent body.  
607 *Sci. Adv.* **6**, eabb1166 (2020).
- 608 35. Oran, R., Weiss, B. P. & Cohen, O. Were chondrites magnetized by the early solar wind?  
609 *Earth Planet. Sci. Lett.* **492**, 222–231 (2018).
- 610 36. Oran, R. *et al.* Maximum energies of trapped particles around magnetized planets and  
611 small bodies. 1–23.
- 612 37. Sridhar, S., Bryson, J. F. J., King, A. J. & Harrison, R. J. Constraints on the ice  
613 composition of carbonaceous chondrites from their magnetic mineralogy. *Earth Planet.  
614 Sci. Lett.* **576**, 117243 (2021).
- 615 38. Morbidelli, A., Bottke, W. F., Nesvorný, D. & Levison, H. F. Asteroids were born big.  
616 *Icarus* **204**, 558–573 (2009).
- 617 39. Maurel, C. *et al.* Meteorite evidence for partial differentiation and protracted accretion of  
618 planetesimals. *Sci. Adv.* **6**, 1–10 (2020).
- 619 40. Elkins-Tanton, L. T., Weiss, B. P. & Zuber, M. T. Chondrites as samples of differentiated  
620 planetesimals. *Earth Planet. Sci. Lett.* **305**, 1–10 (2011).
- 621 41. Fu, R. R. & Elkins-Tanton, L. T. The fate of magmas in planetesimals and the retention of  
622 primitive chondritic crusts. *Earth Planet. Sci. Lett.* **390**, 128–137 (2014).
- 623 42. Bryson, J. F. J., Neufeld, J. A. & Nimmo, F. Constraints on asteroid magnetic field  
624 evolution and the radii of meteorite parent bodies from thermal modelling. *Earth Planet.*

- 625 *Sci. Lett.* **521**, 68–78 (2019).
- 626 43. de Leuw, S., Rubin, A. E., Schmitt, A. K. & Wasson, J. T.  $^{53}\text{Mn}$ – $^{53}\text{Cr}$  systematics of  
627 carbonates in CM chondrites: Implications for the timing and duration of aqueous  
628 alteration. *Geochim. Cosmochim. Acta* **73**, 7433–7442 (2009).
- 629 44. Suttle, M. D., King, A. J., Schofield, P. F., Bates, H. & Russell, S. S. The aqueous  
630 alteration of CM chondrites, a review. *Geochim. Cosmochim. Acta* **299**, 219–256 (2021).
- 631 45. Fu, R. R. & Weiss, B. P. Detrital remanent magnetization in the solar nebula. *J. Geophys.*  
632 *Res. Planets* **117**, (2012).
- 633 46. O’Brien, T. *et al.* Arrival and magnetization of carbonaceous chondrites in the asteroid  
634 belt before 4562 million years ago. *Commun. Earth Environ.* **1**, 1–7 (2020).
- 635 47. Corrigan, C. M. *et al.* The porosity and permeability of chondritic meteorites and  
636 interplanetary dust particles. *Meteorit. Planet. Sci.* **32**, 509–515 (1997).
- 637 48. Travis, B. J. & Schubert, G. Hydrothermal convection in carbonaceous chondrite parent  
638 bodies. *Earth Planet. Sci. Lett.* **240**, 234–250 (2005).
- 639 49. Hutchison, R., Pillinger, C., Turner, G., Russell, S. & Young, E. D. The hydrology of  
640 carbonaceous chondrite parent bodies and the evolution of planet progenitors. *Philos.*  
641 *Trans. R. Soc. London. Ser. A Math. Phys. Eng. Sci.* **359**, 2095–2110 (2001).
- 642 50. Grimm, R. E. & Mccween, H. Y. Water and the thermal evolution of carbonaceous  
643 chondrite parent bodies. *Icarus* **82**, 244–280 (1989).
- 644 51. Neveu, M., Desch, S. J. & Castillo-Rogez, J. C. Core cracking and hydrothermal  
645 circulation can profoundly affect Ceres’ geophysical evolution. *J. Geophys. Res. Planets*  
646 **120**, 123–154 (2015).
- 647 52. Fujii, M., Sato, H., Togawa, E., Shimada, K. & Ishibashi, J. Seafloor hydrothermal

- 648 alteration affecting magnetic properties of abyssal basaltic rocks: insights from back-arc  
649 lavas of the Okinawa Trough. *Earth, Planets Sp.* **70**, 196 (2018).
- 650 53. Travis, B. J., Bland, P. A., Feldman, W. C. & Sykes, M. V. Hydrothermal dynamics in a  
651 CM-based model of Ceres. *Meteorit. Planet. Sci.* **53**, 2008–2032 (2018).
- 652 54. Hercik, D. *et al.* Magnetic Properties of Asteroid (162173) Ryugu. *J. Geophys. Res.* **125**,  
653 e06035 (2020).
- 654 55. Yada, T. *et al.* Preliminary analysis of the Hayabusa2 samples returned from C-type  
655 asteroid Ryugu. *Nat. Astron.* (2021) doi:10.1038/s41550-021-01550-6.
- 656 56. Villarreal, M. N. Understanding the Interiors of Vesta and Ceres Through Their  
657 Interactions with the Solar Wind. (University of California Los Angeles, 2018).
- 658
- 659